SMAI-JCM
SMAI Journal of Computational Mathematics

Splines for Meshes with Irregularities

Jörg Peters

Volume S5 (2019), p. 161-183.
<http://smai-jcm.centre-mersenne.org/item?id=SMAI-JCM_2019__S5__161_0>

Publication membre du
Centre Mersenne pour l'édition scientifique ouverte
http://www.centre-mersenne.org/

Sousmission sur https://smai-jcm.math.cnrs.fr/index.php/SMAI-JCM

SMAI Journal of Computational Mathematics
Vol. S5, 161-183 (2019)

Splines for Meshes with Irregularities

Jörg Peters [1]

[1] Dept CISE, University of Florida, Gainesville FL 32611-6120, USA
E-mail address: jorg.peters@gmail.com.

Abstract. Splines form an elegant bridge between the continuous real world and the discrete computational world. Their tensor-product form lifts many univariate properties effortlessly to the surfaces, volumes and beyond. Irregularities, where the tensor-structure breaks down, therefore deserve attention – and provide a rich source of mathematical challenges and insights.

This paper reviews and categorizes techniques for splines on meshes with irregularities. Of particular interest are quad-dominant meshes that can have $n \neq 4$ valent interior points and T-junctions where quad-strips end. "Generalized" splines can use quad-dominant meshes as control nets both for modeling geometry and to support engineering analysis without additional meshing.

2010 Mathematics Subject Classification. 65N35, 15A15.

Keywords. splines, irregular, classification.

1. Introduction

The *spline control net* forms an intuitive geometrical bridge connecting the essentially discrete world of meshes to the continuum of geometric modeling and analysis: the vertices of the control net are the coefficients of B-splines in the linear combination that forms the spline; and since the basis of B-splines form a non-negative partition of 1, the control net outlines the spline's shape.

This paper focuses on surfaces generated by generalized splines, short *G-splines*, whose control nets form quad(-rilateral) meshes with *irregularities*. Irregularities encompass *extraordinary* mesh nodes where less or more than four quads meet and *T-junctions* where a quad-strip ends and two finer quads meet a coarser one at a node (a T-node). These generalized quad-meshes are still structured in the sense that irregularities are expected to be few and not concentrated near each other.

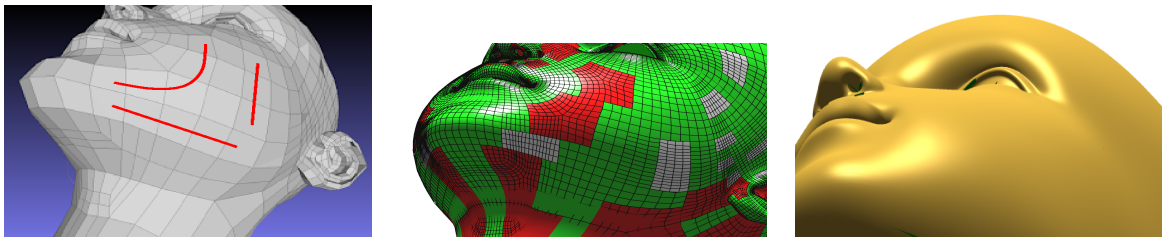

(A) faceted model (B) BB-nets (C) G-spline surface

FIGURE 1.1. Irregularities in a surface model. (A) T-junctions under the chin, an extraordinary point inside the red curve. (B) A generalized spline surface using the mesh in (A) as control net to generate smoothly joining regular bi-3, multi-sided extraordinary and T-junction patches in Bernstein–Bézier (BB) form. (C) smooth rendering of the generalized spline.

supported by Darpa TRADES.

Overview and Disclaimer. The material is based on a presentation at the 9th International Conference on Curves and Surfaces in Arcachon, France. While the paper aims to clarify recent concepts and constructions, it makes no claim to provide an exhaustive survey of spline-based curves and surfaces. Rather the paper emphasizes concepts and results that the author considers valuable and is very familiar with. Hence the reference list is biased towards the author's own work.

Section 2 motivates and illustrates the use of splines on meshes with irregularities and Section 3 is a brief review of basic notions and concepts for splines on meshes with irregularities. The centerpiece of the paper is a classification of splines on meshes with irregularities in a Venn diagram (Figure 4.1). This classification is followed by highlights of the state-of-the-art. Section 4.1 discusses some pros and cons of the dominant trimmed NURBS representation, Section 4.2 surveys some recent progress in smooth surface constructions via the concept of geometric continuity. This is followed by several key facts and a brief review of literature of the three singularly-parameterized classes of polynomial G-splines: Section 4.3 the subdivision surfaces (face collapse), Section 4.4 the polar surfaces (edge collapse) and Section 4.5 the singular jet surfaces (collapse of the low-order Taylor expansion at a vertex). Section 5 concludes with a look at solving higher-order differential equations on G-spline manifolds.

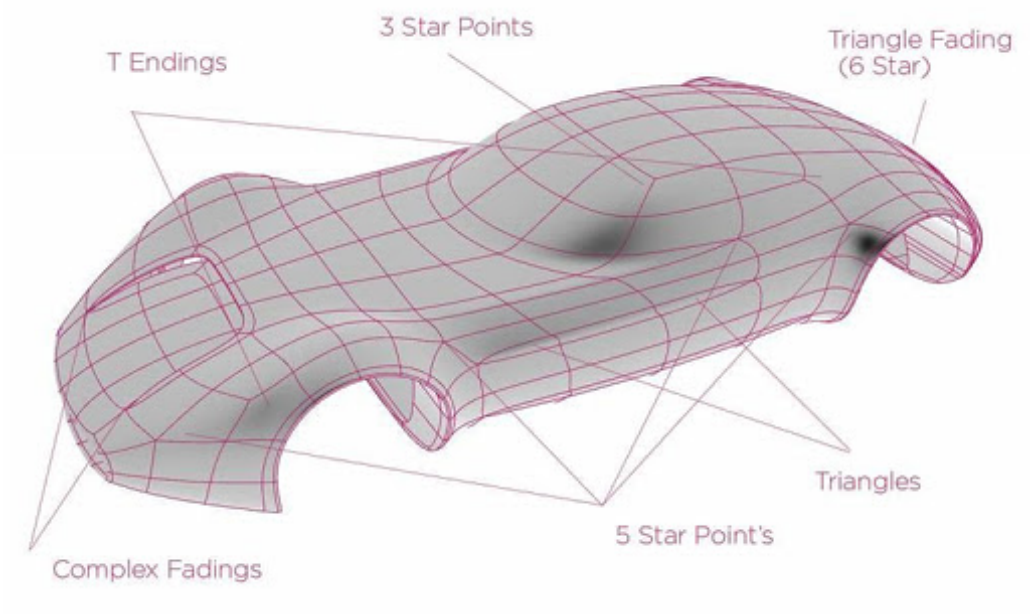

FIGURE 1.2. Irregularities in a faceted automobile design sketch (courtesy S. Eberwein; The control net has been mapped onto a Catmull–Clark subdivision surface).

2. Why splines for meshes with irregularities are needed

While Euler's formula for quad meshes implies the existence of a minimal number of irregularities that varies according to the topological genus, the majority of irregularities in faceted (polygonal, polyhedral) modeling serve to align the mesh with feature and curvature lines. For example, in the faceted model of a girl's head in Figure 1.1 (A), several T-junctions provide varying feature density (near the ear and under the chin) and extraordinary nodes allow a transition between different preferred parameter lines (circular around the mouth to the rectangular partition aligned with the cheek bones). Used as a G-spline control net, the mesh in Figure 1.1 (A) defines the G-spline surface of Figure 1.1 (C). Figure 1.1 (B) shows the partition of this G-spline surface into polynomial pieces. The finer meshes

are the *BB-nets* [14] that connect the coefficients of a patch in tensor-product Bernstein–Bézier form (*BB-form*) [18]. In the design study shown in Figure 1.2, the irregularities are strategically placed and labelled by the designer: the irregularities enable changes in parameter direction (extraordinary points) and density (T-junctions). Just as for a standard tensor-product spline, the G-spline surfaces follow the mesh, interpreted as a control net.

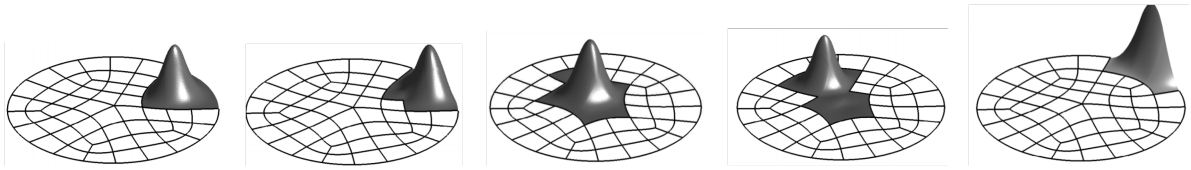

(A) valence $n = 3$ (B) near $n = 3$ (C) near $n = 5$ (D) near $n = 5$ and $n = 3$ (E) boundary G-spline

Figure 2.1. Some piecewise polynomial G-spline basis functions: *the quad-meshes act as G-spline control nets*, i.e. the figures show the result of lifting exactly one quad-mesh node (not shown) out of the plane of the disk.

Figure 2.1 shows several G-spline basis functions with abscissae placed on a planar disk. The spread-out tail in Figure 2.1 (D) serves to include information from all five neighbor quads of the $n = 5$-valent mesh node. Only where the mesh admits a directional decomposition of the smoothness constraints, namely for tensor-product configurations, is the familiar smaller footprint of tensor-product NURBS possible.

A first advantage of using G-splines is their ability to capture smoothly curved shape. This ability is not just important for aesthetic purposes; it also diminishes the error inherent in any faceted approximation: the splines' ability to non-linearly expand towards the true shape deliver higher approximation order. Conversely, spline surfaces can use far fewer elements to represent curved geometry or to guarantee accurate numerical solutions than their linear straight-edge counterparts.

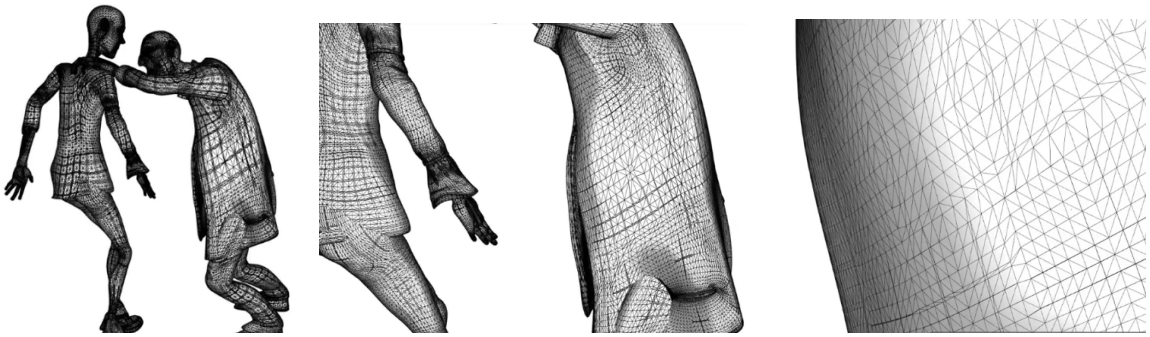

(A) (B) (C)

Figure 2.2. Splines allow infinite resolution under zoom. The scene uses models and is an adaptation of Blender's opensource movie "Elephant's Dream".

A second desirable effect of associating G-splines rather than a fixed triangulation with a mesh is infinite resolution towards the curved shape. Figure 2.2 is a frame from an adaptation of Blender's first opensource movie "Elephant's Dream" [19]. Based on tight *slefe* estimates of spline curvature [67, 85, 86], the tessellation factor is set automatically to ensure pixel-accurate rendering [110] at interactive speeds. That is the silhouettes are always smooth at pixel-resolution and the adaptive triangulation

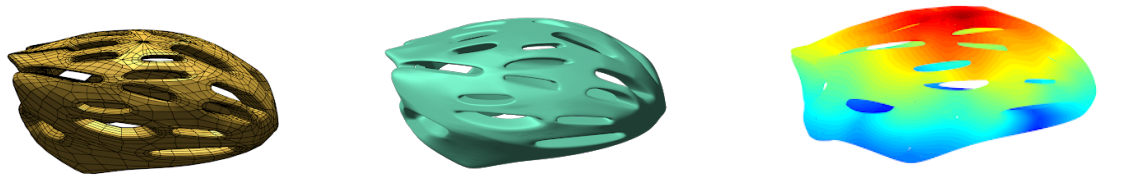

(A) G-spline control net (B) spline surface (C) heat propagation on surface

FIGURE 2.3. G-splines allow direct engineering analysis as finite elements in Galerkin's setting. An additional coordinate at each point of the control net provides degrees of freedom (here to compute the heat propagation on a bicycle helmet under the Florida sun).

provided by the OpenGL or similar graphics pipeline's tessellation engine enables accurate per-pixel lighting. This performs well also in industrial codes [21].

A third desirable feature of G-splines is that (the coordinates of) their control net nodes can be used both for modeling geometry and as coefficients of functions on the surface, e.g. as degrees of freedom for engineering analysis [26]. Especially when the net is refinable and the spline spaces are nested, computing with the control net avoids imprecise and costly re-approximation or conversion, say to a triangulation. G-spline can therefore support an efficient and high-precision design-and-analysis cycle. In particular, for differential equations requiring higher-order continuity, e.g. Kirchhoff–Love shell problems, G-splines offer a smooth and graded parameterization for stability and convergence of solvers. Figure 2.3 shows the progression from a G-spline control net, to modeling the smooth surface, to computing heat propagation on the helmet's surface by employing the one family of splines both for the shape and the temperature function.

3. Basic Notions and Concepts

Both mathematical and aesthetic concepts enter into surface modeling. Stylists, the professionals who translate high-end design into computer-based models, focus on the shape of surfaces via visualization.

Aesthetic assessment. *Highlight lines* [6] are a commonly-used tool of surface interrogation; highlight lines approximate the effect of parallel arrangement of tube lights in an automobile show room, see Figure 3.1(A). They differ from reflection lines in that the observation point is fixed. Unless explicitly intended as a surface feature, abrupt changes in the highlight line distribution are undesirable, because distorted reflections make the product appear less carefully engineered. Uniform, parallel highlight lines can qualify a surface as "class A". Plotting the (normal) curvature along planar cuts, so-called *curvature profiles*, yield an alternative tool to detect oscillations.

"Class A surface" is a term in the automotive design industry [105], describing spline surfaces with aesthetic, non-oscillating highlight lines. "Class A" surfaces satisfy, depending on the application area and contractual agreement, certain hard geometric constraints [1]. In particular, they allow, due to manufacturing tolerances, a mismatch of normals along a curve between two surface pieces of one tenth of a degree. Of the four constructions displayed in Figure 3.2 only (F) qualifies as "class A". This is remarkable since (F) is the only construction that is not mathematically smooth. Surface (F)

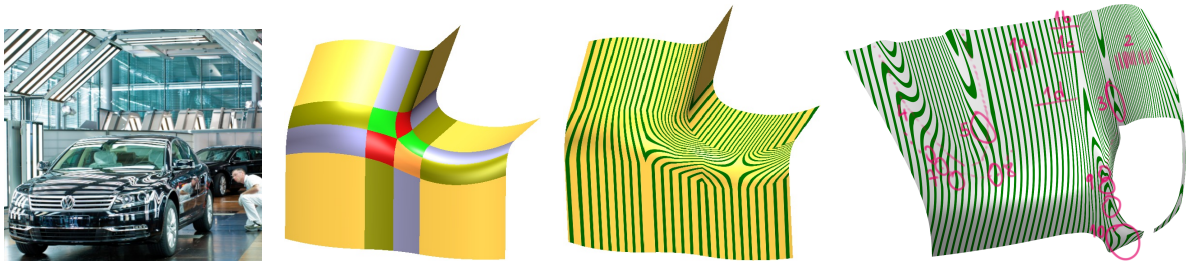

(A) Reflection lines (B) G-spline surface (C) highlight lines (D) quality assessment

Figure 3.1. Judging surfaces by (A) reflections of parallel lights (reflection lines) [13] and (D) highlight lines. (B) Pairwise joined primary surface pieces (patches) capped an *irregular* 5-piece neighborhood. Although the central cap consists of five patches the highlight line distribution (C) is uniform, hence deemed good. (D) Annotation of desirable highlight line distribution (1a,1b,2) and deficient regions (1c,1d,3,4,5,7,8,9,10).

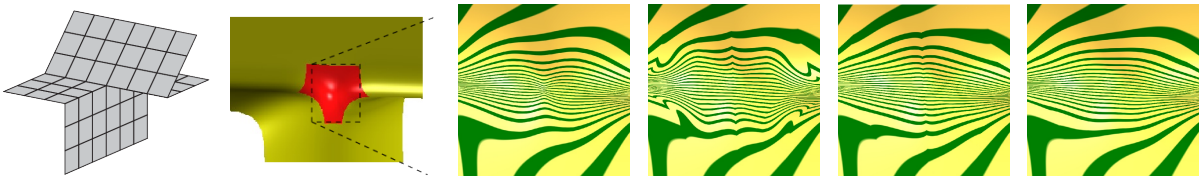

(A) 2-beam join (B) cap (C) Catmull–Clark [10] (D) C^1/G^1 [25] (E) rational [66] (F) $C^{1-\epsilon}$ [45]

Figure 3.2. "Class A" surfaces avoid oscillating highlight lines but allow a mismatch of normals up to 1/10th of a degree. The input mesh (A) models two crossing beams whose join is to be smoothed by a bi-3 a multi-sided spline cap (red in (B)). The cap is enlarged in (C)–(F) for four alternative constructions. Remarkably only the mathematically non-smooth spline surface (F) qualifies as "class A".

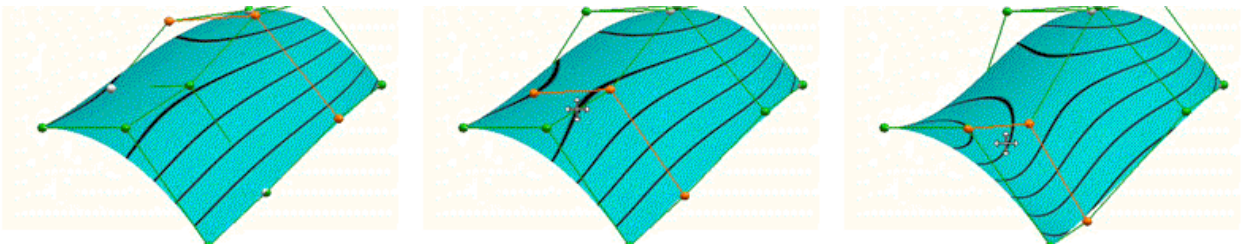

Figure 3.3. Interactive surface styling [106]: manipulating the highlight line distribution by moving BB-coefficients requires experience.

has a mismatch of normal where patches join of up to 1/10th of a degree, but also a good highlight line distribution. Evidently "Class A" differs from the mathematical notion of smoothness.

Irregularities. Irregularities in quad meshes arise by design as in Figure 1.2. They also arise when reconstructing scanned data with quad-meshing algorithms [8, 102]. We distinguish two types of irregularities: extraordinary points and T-junctions. Each mesh extraordinary node where $n \neq 4$ quads meet corresponds to an *extraordinary point* where n four-sided surface patches meet. The extraordinary points can be "star-like" or "polar", see Figure 3.4. If we think of neighborhoods modeled by

conformal maps, star-like neighborhoods are generated by $z^{4/n}$, polar by e^z; lens-shaped, valence $n = 2$ configurations, add maps z^2 and $\cos z$ into the mix [43].

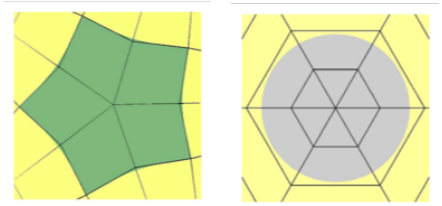

(A) star-like (B) polar

FIGURE 3.4. The two main structures of bivariate extraordinary configurations.

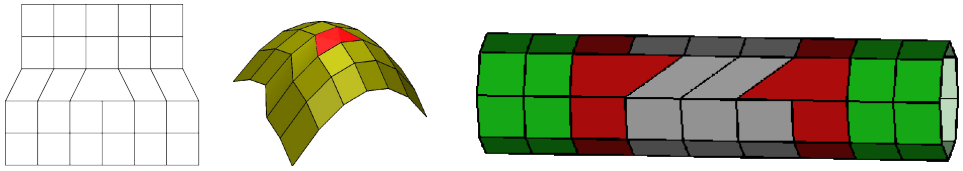

(A) T-net + quad frame (B) convex T-net (C) T-splines fail for this mesh

FIGURE 3.5. (A) and (B) control nets with a single isolated *T-junction. (C) A consistent global knot spacing implies zero horizontal knot intervals for the grey quads and so, formally, the parameterization is not smooth.*

T-junctions occur where strips of surface patches terminate: two finer surface pieces meet one coarser piece. The simplest such configuration, a T-net, is shown in Figure 3.5 (A): a nominally pentagonal face with exactly one vertex of valence 3 is surrounded by quadrilateral facets (here with a second frame of quads for surface context). T-junctions allow introducing geometry of higher detail, or to merge two separately-developed spline surfaces. T-junctions prominently arise when replacing the global constraints of strict quad-meshing by more flexible quad-dominant meshing [31, 76, 89]. T-junctions also appear to hierarchical splines [16, 20, 33, 60, 96] (and hence subdivision surfaces). However, T-junctions in hierarchical splines require discovering a globally consistent choice of knot intervals. For a given quad-mesh with irregularities, such a choice of knot intervals may fail to exist. For example, if we require that the sum of knot intervals on opposing edges of any face must be equal (Rule 1 of [96]) then the horizontal knot intervals of the grey helical strip must be zero in Figure 3.5 (C) so that no smooth spline parameterization exists. Unsurprisingly, current industrial implementations of T-splines (Rhino, Autodesk) do not try to recognize T-junctions in input meshes but treat them as 3-valent nodes. Generally, hierarchical splines are intended to *create T-junctions* as part of a refinement process where knot interval consistency is guaranteed. By contrast, the G-splines covering the T-junctions for "class A" modeling [55], as in Figure 1.1 (B) are not concerned with or restricted by knot spacing.

Trimming. Restricting the domain of a spline by curves in u, v space, is called trimming. In high-end design, primary surfaces are juxtaposed and their sharp transitions blended by fillets. The switch from primary to fillet surface or between primary surfaces is then traced back to trim curves in the domain. This reflects the traditional work flow of design using clay [107] and is a basic element of leading high-end design software. In state-of-the-art styling software polynomial pieces in Bernstein–Bézier form (BB form) are laid down to capture primary shape and then cut back (aka trimmed) to insert

fillets between the primary surfaces. This technique preserves simple, elegant shape in the large and is initially very efficient – however later in the modelling process stylists devote more and more time on ever smaller blends between the primary surfaces.

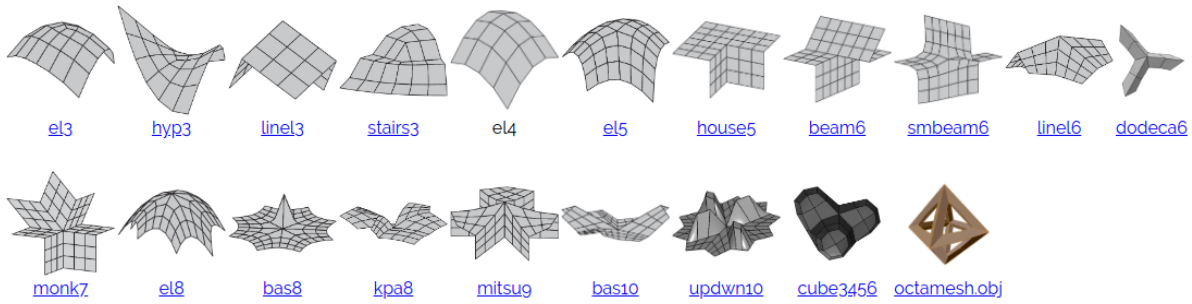

Figure 3.6. Part of an obstacle course of challenging quad-net inputs.

A G-spline obstacle course. Since "class A" criteria are subjective, the quad-net obstacle course [38] provides input meshes in .obj format that can be used to test G-spline algorithms on common and less common hard inputs Figure 3.6.

4. Classification

There are many criteria to classify free-form surface representations: CAD compatibility, polynomial degree, approximation order, etc.. The Venn diagram Figure 4.1 groups by smoothness, polynomiality and singularity of the surface parameterization. The topmost entry, *trimmed NURBS* surfaces, is the de facto industry standard. Section 4.1 discusses advantages and shortcomings of trimmed NURBS surfaces that have motivated research into alternatives over the last 30 years. The two best-known alternatives are geometrically smooth G^k constructions, discussed in Section 4.2, and the hierarchical refinement by subdivision surfaces, discussed in Section 4.3. But to date neither has replaced trimmed surfaces in high-end manufacturing design.

Conforming C^0 surfaces, including curved triangulations, are ubiquitous in low-end engineering analysis and computer graphics. In computer graphics, a particular type of trompe l'oeil is often used to generate the appearance of smoothness when the computational overhead must be minimized: taking advantage of the separate channels for position and normal in the graphics pipeline, the constructions of [103, 80, 63, 28] pair each surface patch with a related but independent normal distribution "patch" to be used for lighting computations. Except for some silhouettes, the visual appearance then is smoother than that of the true geometric shape. Importantly the trompe l'oeil can be computed on the fly in the graphics processing unit (GPU) pipeline with negligible overhead compared to the original faceted representation.

$C^{1-\epsilon}$ constructions acknowledge the preference of "class A" surfacing for good highlight line distribution over strict mathematical smoothness. Typically, large portions of surfaces are of degree bi-3 but the polynomial degree needs to increase near irregular points. By accepting a slight error in one or more algebraic mathematical smoothness constraints, constructions like [45] achieve good highlight line distributions. And the mismatch of normals is bounded below one tenth of a degree over the obstacle course, Figure 3.6. The "class A" surface tolerances can so be met by polynomials of degree of bi-3 everywhere, see e.g. Figure 3.2(E).

Generalized barycentric patches, e.g. [64, 99], and non-4-sided *transfinite constructions*, e.g. [11, 91, 92, 100, 101], yield internally infinitely smooth multi-sided patches (see [27] for efficient hardware rendering). Exactly computing their higher-order derivatives is, however, costly due to an underlying very high rational degree; finite difference approximations of the derivatives are therefore often used instead. Gregory's classic construction [22] induces a second-order rational singularity at each corner and so allows independent definition of mixed derivatives across two edges meeting at the vertex. Barycentric, transfinite, Gregory and orbifold constructions are, undeservedly, not further discussed below.

The three *singular polynomial constructions* are: collapse of patch size (subdivision surfaces, Section 4.3), collapse of edges to a pole (polar surfaces, Section 4.4), and collapse of the Taylor expansion at a vertex (singular jet surfaces, Section 4.5). The third notably generalizes to $m > 2$ variables, e.g. to splines on hexahedral complexes with irregular vertices and irregular edges [82].

Note that the Venn diagram regions for smooth constructions overlap since constructions can borrow features from each other: for example, [29] shows that "barycentric" and the "Gregory" approach are not mutually exclusive, and Section 4.3 will suggest that it makes sense to combine a few steps of (accelerated, guided) subdivision with a G-spline construction.

The classification omits smooth piecewise polynomial functions on triangulations. These can also be used for engineering analysis [32] and are summarized in the seminal book [95] by Schumaker and Lai.

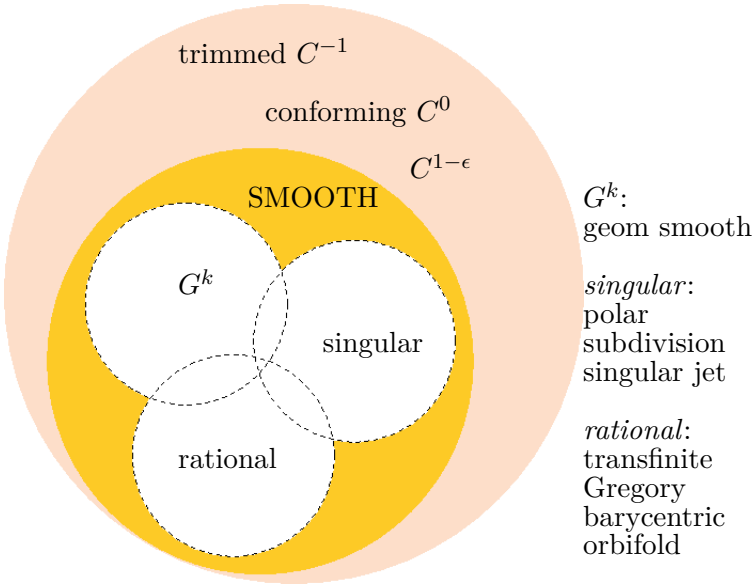

FIGURE 4.1. Major categories, arranged by smoothness, of surface representations for meshes with irregularities. Polar, subdivision and singular jet constructions leverage controlled singularities and can be piecewise polynomial; G^k geometrically smooth constructions, too, can be polynomial and rely on change of parameterization between pieces; orbifold and generalized barycentric constructions use multi-sided domains, and, as do transfinite and Gregory patches, rational blending functions for $n \neq 4$-sided surface pieces.

4.1. **Trimmed Surfaces**

Design is typically hierarchical, starting with a base shape and refining the design by replacing pieces. Trimming accommodates the integration with other design components. The trimmed surface paradigm is powerful in that it allows the designer to freely determine primary shape, then restrict it based on functionality and detail, e.g. to subtract out a cylinder. The resulting boundary representation (B-rep) is mathematically uniform and is efficiently supported by the industry standard of trimmed NURBS (non-uniform rational B-spline).

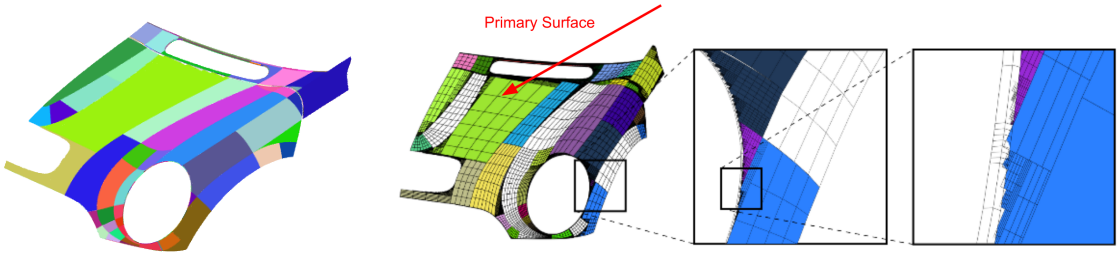

(A) Surface patch layout (B) heterogeneous parameterization and size

Figure 4.2. High-end design emphasizes *shape over parameterization*. (A) Model of a car hood created by automobile stylists using professional software. (B) The control nets of adjacent pieces, indicated as grid lines, are entirely unrelated. Repeated zoom reveals orders of magnitude size differences between the headlight rim (white) and the trimmed-off fender (blue).

Working with synthesized trimmed surfaces, obtained by composition of NURBS, is straightforward since they have a NURBS representation and various approximations can be applied to lower the degree. By contrast, working with surfaces whose trim arises from intersection, as is the focus in this section, is challenging. Such a collection of trimmed splines is typically not even continuous since (the pre-images of) 3D intersection curves are algebraic but generically non-rational and are therefore only approximated by NURBS. The collection of trimmed splines is also typically heterogeneous in size, parameter line orientation and polynomial degree (see Figure 4.2). The corresponding gaps and the anarchic parameterization creates numerous problems for downstream design and analysis. Since smooth and graded parameterizations of the computational domain are indispensable for the stability and convergence of solvers for higher-order partial differential equations at the heart of the engineering process, even minute gaps in trimmed surfaces can result in non-physical solutions. And non-smooth parameterizations can cause spurious solutions when the solution is known to be smooth since the chosen solution space is too large.

Heterogeneity in size, parameter line orientation and polynomial degree forces re-approximation prior to analysis and possibly extensive post-processing. Whole research communities and software suites are devoted to the tricky tasks of "healing" and meshing surfaces to compute with them without reducing the accuracy too much. [68] lists many approaches to dealing with trimmed surfaces (its characterization of the earlier-mentioned approach of [110] as using a "trim texture" is however not accurate).

Often distinct representations are used at each stage of design and simulation, replacing the carefully-designed initial surface by triangles or even axis-aligned voxels for analysis and simulation. This mix of representations is well-known to trigger corrections and adjustments downstream, e.g. prior to manufacturing, and so causes a bottleneck in the design-analysis cycle. This deficiency motivates the following alternative surface representations.

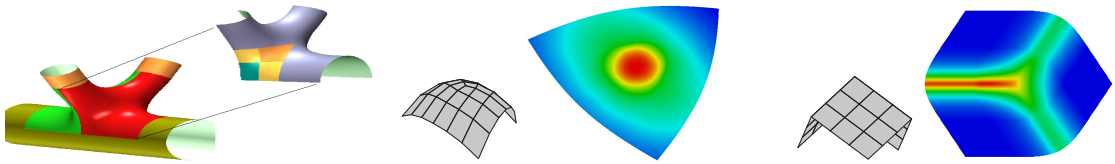

(A) (B) (C)

FIGURE 4.3. Geometrically smooth G^k-surfaces: modeling and interrogation. (B) and (C) Gauss curvature shading from minimal (blue) to maximal (red) gauss curvature.

smooth	regular	irregular	valence	split	reference
C0	bi-3	bi-3	any	2x2	[45]
G1	bi-2	bi-3	3,5		[47]
		bi-4	6,7,...		[47]
		2,4	T_0, T_1, T_2		[57]
	bi-3	bi-4	3,5,6		[36]
		bi-5	7,8,...		[36]
		bi-4	any	2x2	[36]
		3,5	T_0, T_1, T_2		[55]
	bi-3	bi-5	any		[46]
G2	bi-3	bi-6	any		[49]
	bi-3	bi-5		2x2	[44]
		$3,9_6$	T_0, T_1, T_2		[55]
	MSV	bi-4		2x2	[48]
		bi-5			[48]

TABLE 4.1. Recent G^k geometrically smooth constructions with good highlight line distribution verified on the geometric obstacle course [38]. MSV = minimal single valence control mesh; 9_6: the degree 3,6 construction has visually identical curvature images to the degree 3,9 surface.

4.2. **Geometrically smooth, G^k surfaces**

Two surface pieces $\tilde{f}$ and f sharing a curve segment E along their respective edges join G^k if there is a suitably-oriented and non-singular reparameterization $\rho : \mathbb{R}^2 \to \mathbb{R}^2$ so that the jets $\partial^k \tilde{f}$ and $\partial^k (f \circ \rho)$, agree along the curve segment E [23, 81]. In short, derivatives of G^k-joined patches match after a change of variables.

To be compatible with industry standards, geometrically smooth G-splines typically consist of (a finite number of) tensor-product polynomial (or rational) pieces. But they can also be built or combined with total degree (triangular) pieces [78, 79].

Early G^2 constructions used patches of degree bi-18 [24], bi-9 [59, 109], bi-7 [62, 65]. The constructions in [88, 90] achieve bi-6, provided the shape at the extraordinary point is restricted to quadratics. Modern curvature continuous constructions for filling n-sided holes in a bi-3 spline complex have a polynomial degree as low as bi-5 [44] (using a 2×2 arrangement of patches per quad) or bi-6 [44, 49] (using a single patch per quad). Both constructions deliver formally C^2 surfaces and a good highlight line distribution over the geometric obstacle course of challenging inputs of Figure 3.6 [38].

Recent efforts for formally not curvature continuous constructions have focused on optimizing shape rather than only satisfying the algebraic patch transition constraints for smoothness. There are many

different options for geometric G-splines in the literature, as many as there are spline families in the regular case. As listed in Table 4.1, one can classify constructions by the degree of the surface on the regular grid, near irregularities and the recommended maximal valence of the irregular point or type of T-junction. Lower degree can be achieved by $m \times m$ macro-patches per quad sector. Where C^1 continuity of the surface suffices, a good trade-off between polynomial degree and the highlight line distribution over the obstacle course (Figure 3.6) is achieved by G^1-splines such as [47] and [46] (see Figure 4.3). Extensive experiments when deriving geometrically smooth splines indicate that using functionals, such as

$$\mathcal{F}_\kappa f := \int_0^1 \int_0^1 \sum_{i+j=\kappa, i,j\geq 0} \frac{\kappa!}{i!j!} (\partial_s^i \partial_t^j f(s,t))^2 \mathrm{d}s\mathrm{d}t,$$

$$\mathcal{F}_\kappa^* f := \int_0^1 \int_0^1 (\partial_s^\kappa f(s,t))^2 + (\partial_t^\kappa f(s,t))^2 \mathrm{d}s\mathrm{d}t$$

are useful when applied to maps $\mathbb{R}^2 \to \mathbb{R}^2$, e.g. when optimizing sampling in the domain. However these functionals only rarely, and then unpredictably, yield good highlight line distributions for surfaces embedded in $\mathbb{R}^3$ [44].

While geometrically smooth G-splines excel in shape, they lack simple refinability. De Casteljau splitting of the pieces in BB-form [14, 18] does not provide refined *smooth spaces* with additional degrees of freedom. To understand the problem observe that when refining a G^1 construction, the influence of the irregularities shrinks so that more remote parts of the initial reparameterization edges look regular to a local spline construction and are, by default, joined with parametric C^1 smoothness rather than the original G^1 smoothness. Since spaces with different smoothness are not equal, representation of geometry (or analysis functions on the G-spline surface) are not nested: the finer representation cannot reproduce the coarser unless it keeps track of all G^1 transitions (see [51] for the resulting complex distribution of unrestricted control points in a reproducing refined G-spline representation).

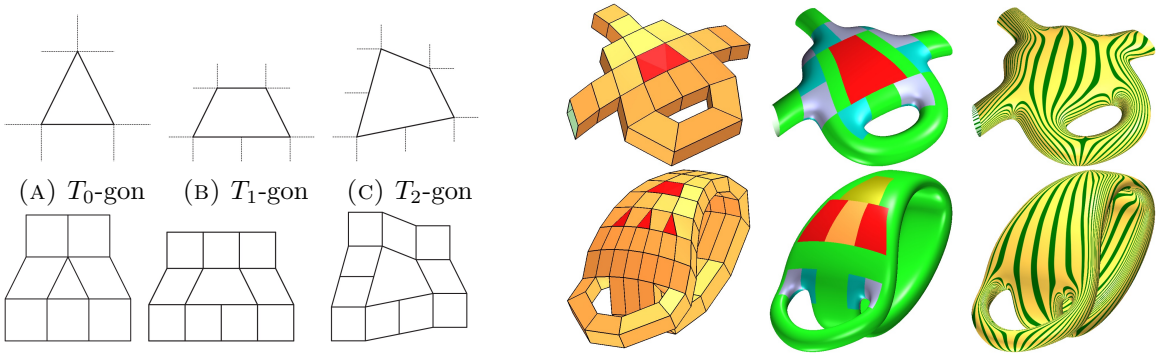

Figure 4.4. T-gons and τ-configurations. (A–F) The subscript counts the number of T-junctions. (G,H,I) Using τ-configurations as parts of control nets. (G) Mesh with T-gons and irregular nodes of valences 3 and 5. (H) Patch layout: regular bi-3 patches; τ-spline surface (also orange and yellow where they are close together) and multi-sided caps (grey or blue). (I) Smooth highlight lines across the patch complex.

Only recently have n-gons with **T-junctions** (T-gons) in unstructured quad-dominant meshes been recognized as a distinct challenge for G-splines. A single T-junction represents a change of quad-strip density in one direction (and no change in the other). While G-splines for multi-sided holes can, in

principle, smoothly cover τ-nets, they are direction-agnostic. By not preserving the two preferred directions (of change and no change) they can cause visible shape artifacts. Constructions for τ-nets naturally reparameterize (along) the direction of change. Subtly different constructions are best for different polynomial degree of the regular spline complex (e.g. bi-2 [57] or bi-3 [37, 55, 56]), for ease of refinement, quality of the resulting surface ([55] vs [37]) and the locality of the constructions ([56] vs [37]).

Admissible control nets for current (tensor-product) G-splines have a succinct characterization as *locally quad-dominant*: all non-4-sided facets must be surrounded by quadrilaterals.

We close by noting that the cost of *construction and evaluation of G^k splines* is comparable to converting a tensor-product NURBS patch to BB-form (a matrix multiplication) and then evaluating the pieces in BB-form. The G-spline control net therefore provides simple, efficient degrees of freedom for analysis and optimization (see Section 5).

(A) nested sequence of rings (B) control points

FIGURE 4.5. Subdivision as a sequence of nested surface rings.

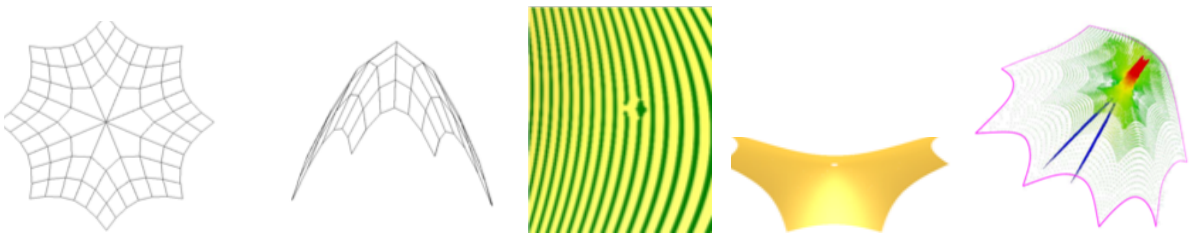

(A) convex input (B) highlight flaw (C) limit shape (D) Gauss curvature needles

(E) flat region from T-junction mesh (F) pinched highlight lines

FIGURE 4.6. Flaws of Catmull–Clark subdivision. *top* row, (A-D): For $n > 4$, the two subsubdominant eigenfunctions of Catmull–Clark subdivision are both saddle-shaped. Therefore even convex inputs yield saddle in the limit. (E) T-junctions break into a 3-valent and a 5-valent neighborhood and induce flatness. (F) Higher valence easily leads to pinched highlight lines.

We next look at three families of singular constructions whose C^k transitions between patches offer simple

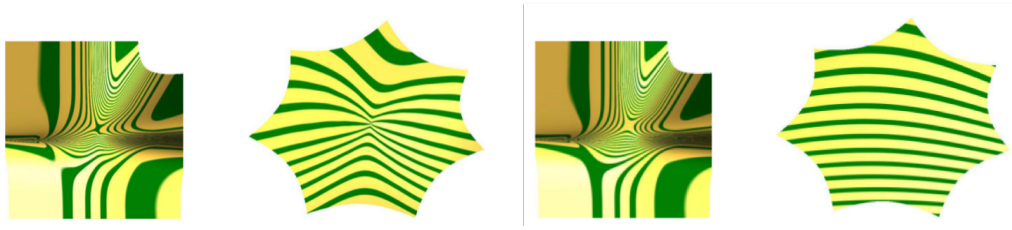

(A) Catmull–Clark (B) Guided Subdivision

Figure 4.7. Catmull–Clark vs. Guided Subdivision

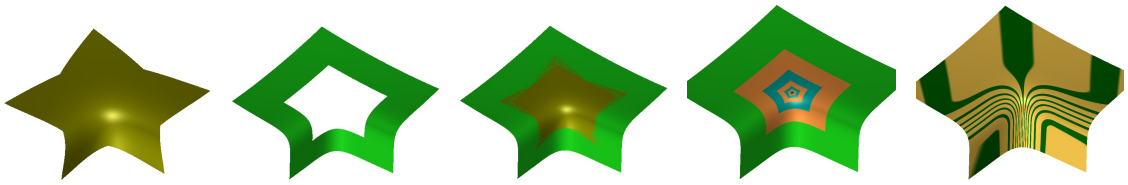

(A) guide surface (B) regular ring (C) mismatch (D) resolution (E) highlight lines

Figure 4.8. Guided Subdivision. At each step, the control points yield a ring whose free inner coefficients are set by the guide shape.

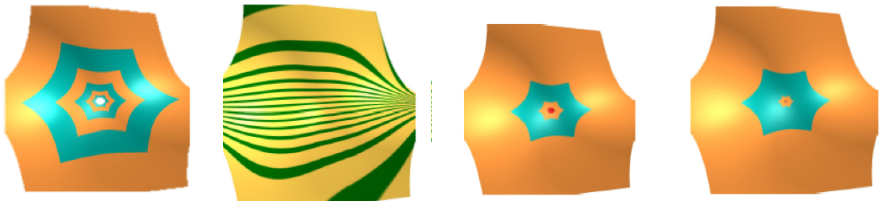

(A) 6 rings + cap (B) shared highlight lines (C) 3 rings, double speed (D) 3 rings, yet faster

Figure 4.9. Accelerated Guided Subdivision: all three surfaces have visually the same highlight line distribution shown in (B).

4.3. **Subdivision Surfaces**

Subdivision surfaces consist of a sequence of contracting nested surface rings (see Figure 4.5(A)) that provide an ever finer approximation of their limit. Catmull–Clark subdivision [10] is widely used in the entertainment industry [15] and is convenient for conceptual design (Figure 1.2). Besides natural refinement, a major appeal of subdivision are its simple rules, called stencils, that describe how a new finer mesh is derived from a coarse outline. Due to the singular limit, a complete mathematical analysis of such surfaces is non-trivial [17, 84].

However subdivision schemes governed by simple stencils do not meet the "class A" requirements. Detailed analysis as well as test cases in [58, 50] have exposed major shape deficiencies. Figure 4.6 shows three types of flaws: (A) saddles arising in the limit from convex input nets for valence above $n = 4$, (B) unwanted flatness due to neighboring extraordinary points and (C) pinched highlight line distributions for higher-order saddles. These shape defects preclude the use of classical small-stencil subdivision for "class A" surface constructions. Moreover, the infinite recursion complicates their inclusion into existing industrial design infrastructure. In particular, special techniques are needed to

correctly compute integrals near their irregularities as is needed for populating the governing equations, say of elasticity [73, 4, 5].

Guided Subdivision [40] is an effective tool to overcome the defects of standard subdivision algorithms (Figure 4.7). Moreover, unlike standard subdivision, guided subdivision can generate curvature continuous subdivision surfaces. Figure 4.8 illustrates the underlying principle: the control mesh yields both (A) a guide surface and (B) a (sequence of) surface ring(s). Since the guide surface and the surrounding surface frame do not fit together (C), the subdivision step retains the outer part of the ring (that fits its predecessor ring) and determines its new inner part by sampling the guide (D). Remarkably the overall process is linear and stationary and can so be interpreted as subdivision with large stencil, i.e. with a denser subdivision matrix than Catmull–Clark subdivision. While the rules become more complex, the mathematical analysis of the limit becomes much simpler – and the shape is far better [54].

While guided subdivision improves shape, it does not address the problem of infinite recursion. Stopping the recursion after a few steps and filling the remaining hole with multi-sided facet leads to noticeable flaws in the highlight line rendering. A better solution is to fit an n-sided G^1-cap. Since the resulting surface consists of a fixed number of surface pieces, it is industry compatible. To combine the best features of subdivision and geometrically continuous surface constructions one can observe that in practice, design and analysis work with a maximal anticipated level of refinement. When the maximal anticipated refinement level at the irregularity is realized by the cap, it need not be refined and refinement in the surrounding finite coarser surface requires only standard spline knot insertion [52].

Moreover, since guided subdivision stabilizes the shape, an additional technique can be leveraged: *accelerated* guided subdivision [83, §5], [53] widens the surface rings and so achieves a more rapid contraction of the remaining gap (Figure 4.9). When the surface rings and final cap follow a guiding shape, good highlight line distributions are obtained for the shape obstacle course, already when the accelerated sequence of C^k-joined surface rings is G^1 completed after 2 or 3 rings, see Figure 4.9 (B).

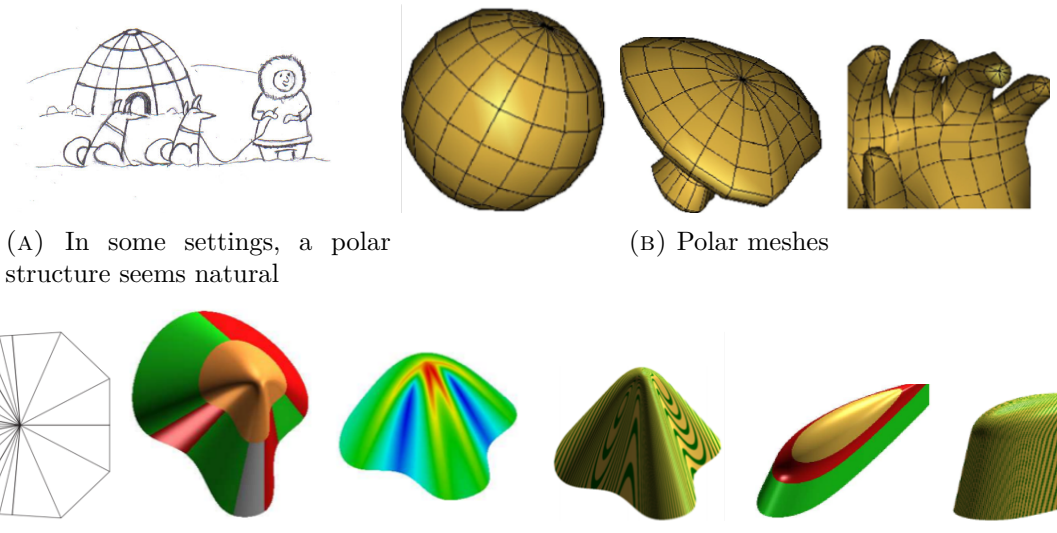

(A) In some settings, a polar structure seems natural

(B) Polar meshes

(C) Polar Surfaces

FIGURE 4.10. Polar meshes and surfaces.

4.4. **Polar constructions**

Polar constructions collapse an edge to the extraordinary point called pole, both for subdivision surfaces [34, 39, 71] and for finite constructions [41, 42, 69, 70, 72, 97]. Some typical polar meshes are shown in Figure 4.10 (A) and (B). Polar constructions work well where a high number of surface pieces join; in fact their shape improves with valence whereas that of star-shaped constructions deteriorates with higher valence [83]. Notably, Catmull–Clark subdivision surfaces visibly oscillate for a cylinder mesh whose top cycle is collapsed to a high-valent pole. By contrast, polar subdivision [71] achieves not only good shape at the pole, but yields a C^2 subdivision such that the rings are all degree bi-3. C^2 subdivision with pieces all of degree bi-3 is noteworthy since in the star-shape setting, obtaining a C^2 subdivision with rings of degree bi-3 is a long-unsolved problem (see [83, Sect 5] for an unorthodox earlier solution).

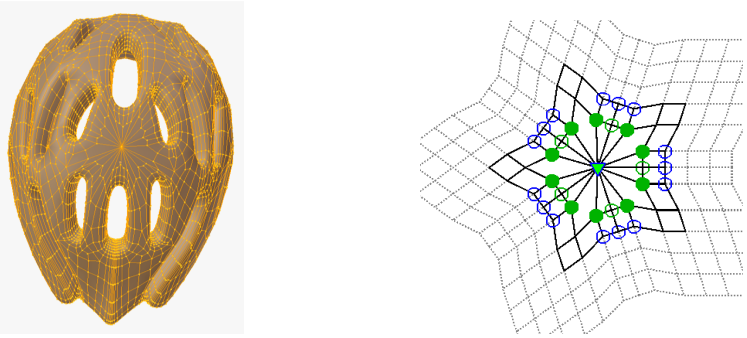

(A) helmet mesh

(B) central BB patches with collapsed first-order jet

Figure 4.11. A singular jet surface. (A) The construction is robust: even the central vertex of valence $n > 20$ on top of the helmet mesh is admissible and does not prevent engineering analysis [75]. (B) BB-net for five sectors.

4.5. C^1 **singular jet surfaces**

Representations with forced singularities by *coalescing control points* (collapsing the control net) [77, 87] have recently shown promise for engineering analysis [75]. The construction collapses the first-order jet and then projects the lowest-order non-zero expansion terms at the irregular point into a fixed plane. [75] associates with each irregular quad not just one but four polynomial pieces. This localizes the construction, allows irregular points in close proximity and yields, for every regular or irregular input quad, exactly 2×2 degrees of freedom with corresponding linearly independent functions. Figure 4.11 (B) illustrates the construction: The central point is the superposition of all BB-coefficients in a 1-neighborhood of the central point. The BB-coefficients marked as • lie in one plane. Regular C^1 constraints determine the BB-coefficients marked ○ and ○. Remarkably, the construction generalizes to higher dimensions, e.g. to unstructured hex-meshes [82]. For surfaces, the shape of singular corner surfaces near the irregular point is typically poor, but can be improved using a guide surface and refinement (Figure 4.12, [50]).

5. **Higher-order engineering analysis on G-spline surfaces across irregularities**

When both geometry and functions on the geometry are piecewise linear then *iso-parametric* analysis is a standard tool for solving differential equations. But if the correct solution space contains only

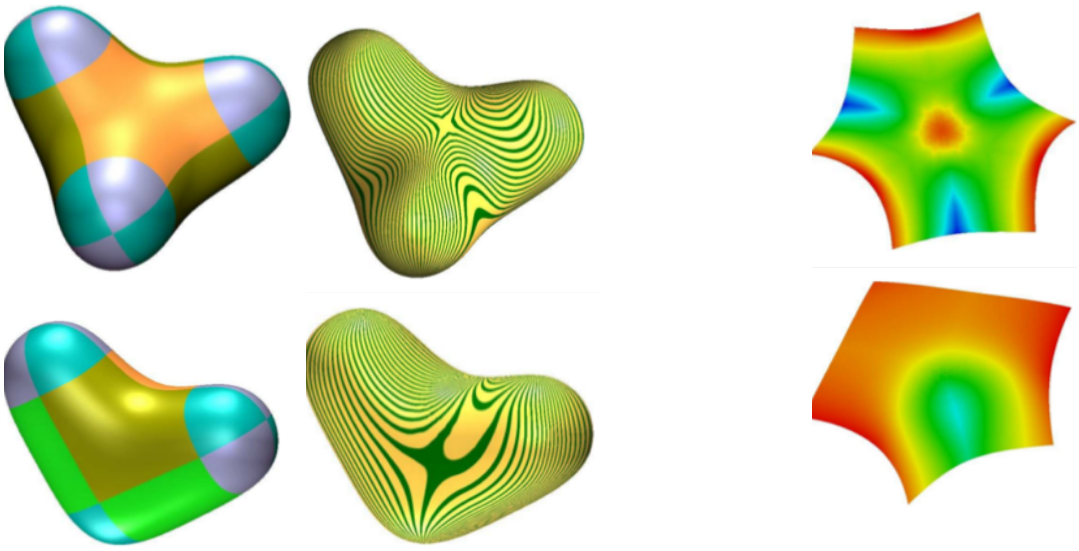

(A) Valence 3,4,5,6

(B) Gauss curvature

FIGURE 4.12. Improved shape of singular corner surfaces via the guided approach [50].

smooth functions, C^0 finite elements even of higher order represent too large a space that can result in extraneous solutions that do not correspond to physical solutions. For example, fluid flows computed with the Discontinuous Galerkin approach can have jumps in the flow lines. Higher-order differential equations such as the biharmonic equation, Kirchhoff–Love shell simulations (Figure 5.1), or simplified Navier–Stokes–Korteweg equations require C^1 finite elements even when using the Galerkin formulation.

The practice of using bi-variate splines, both for modeling the geometry of the domain and for computing functions on this domain *without irregularities* goes back at least to the 1980s [9] and has been regularly advocated and advanced in the literature [2, 3, 94, 98] and embodied in industrial code (see Boeing's "geoduck" analysis software). Similarly, subdivision surfaces have been leveraged both for modeling geometry and engineering analysis [12]. The goal of this approach is to use the exact geometry models of CAD systems directly for numerical simulations without conversion to secondary meshes. That is one aims at discretizing and solving partial differential equations on the geometry by splines of the same type (and their refinement by knot insertion). To emphasize the use of B-splines for both geometry and analysis, the term *iso-geometric* analysis (IGA) was coined in [30], superseding the names "higher-order", "isoparametric" or "finite elements using NURBS" used in the 1980s and 1990s. While IGA with irregularities has now largely been addressed (see e.g. [12, 35, 73]), the promise of iso-geometric analysis, to use CAD models directly for the numerical simulation, is still not met due to several challenges: 1. Instead of parametrizing the volume, only boundary surfaces of the objects are available; 2. Patches may be trimmed; 3. Gaps, jumps and overlaps may occur (Figure 4.2); 4. Parametrizations vary in density, size and preferred directions.

Untrimmed G-splines automatically yield smooth analysis elements. That is, if the model can be represented by G-splines then a fundamental theorem [26] guarantees that one can directly compute shell and other higher-order partial differential equations on the design geometry without additional meshing or triangulation. Specifically, the necessary and sufficient requirement is that the atlas $\mathbf{x}$ of the physical domain and the analysis function u on the standard domain are from the same G-spline space. For example, if $\mathbf{x}_1$ and $\mathbf{x}_2$ are related by kth order geometric continuity across an interface E (cf. Section 4.2), and the corresponding edges of the domains $\square_1$ and $\square_2$ related by the change

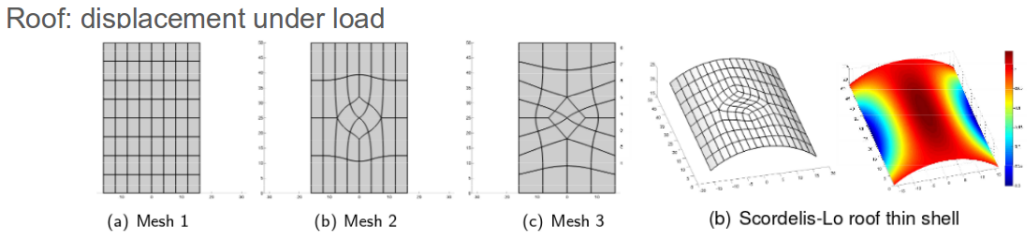

(A) Scordelis–Lo roof

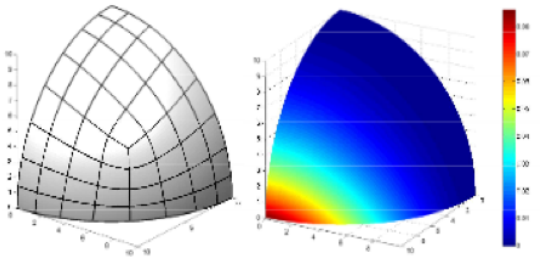

(B) Octant of a sphere

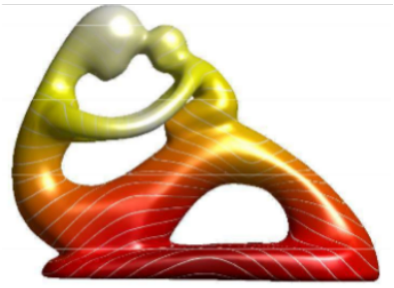

(C) heat propagation

Figure 5.1. Shell displacement and heat propagation computed as G-splines on G-spline surfaces. The quad-meshes act as G-spline control nets. (A) Comparing three different quad-mesh layouts of which two are intentionally irregular to challenge geometrically smooth spline-elements for a benchmark problem of the *shell* obstacle course [7] (B) Stress on a sphere octant. (C) Propagation of heat from its dark red source forms a geodesic parameterization.

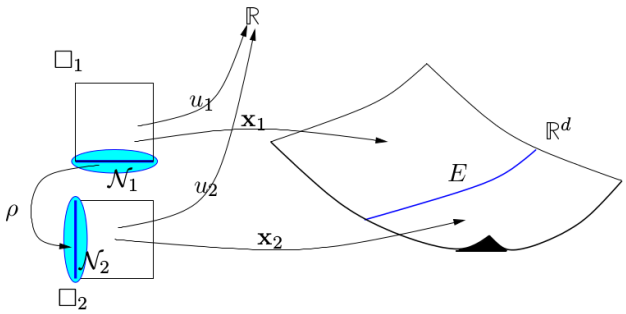

Figure 5.2. Relation of maps in the *fundamental theorem for iso-geometric G-spline elements*: $u_\alpha \circ \mathbf{x}_\alpha^{-1}$, $\alpha = 1, 2$.

of variable ρ, and if u_1 and u_2 are equally related by ρ, i.e. they are matched G-constructions, then $u_1 \circ \mathbf{x}_1^{-1}$ and $u_2 \circ \mathbf{x}_2^{-1}$ are C^k-joined isoparametric elements [26]. An analogous theorem holds for singular constructions. Therefore G-splines not only serve to design the shape controlled by meshes with irregularities but also to directly yield finite IGA elements. These finite elements have been tested on the classical *finite element obstacle course* [7] (see Figure 5.1); [36, 73, 74, 75] for generalized quad meshes, and [32, 61, 104, 108] for other meshes. Recent studies of convergence, [93], focus on the important special case of geometric continuity of graphs of functions.

6. Conclusion

This paper explained and illustrated the need for irregularities in quad-meshes and the corresponding need for generalized splines (G-splines) controlled by meshes with irregularities. A simple Venn-diagram gave a classification of piecewise polynomial (and rational) G-splines. Some of the more recent advances in defining G-splines were illustrated and demonstrated to be usable for modelling and directly, without re-approximation, for engineering analysis.

Acknowledgements

Many of the ideas and algorithms for splines on meshes with irregularities arose in collaboration with Ulrich Reif, Kęstutis Karčiauskas and Thien Nguyen. My thanks go to Malcolm Sabin for reading and commenting on a draft and the organizers of Curves & Surfaces for providing such a good forum for the community.

References

[1] Z. Andjelic. What is the definition of a class A surface? `https://grabcad.com/questions/what-is-definition-of-class-a-surface`, accessed May 2015.

[2] F. T. K. Au and Y. K. Cheung. Spline Finite Elements for beam and plate. *Computers & Structures*, 37:717–729, 1990.

[3] F. T. K. Au and Y. K. Cheung. Isoparametric Spline Finite Strip for Plane Structures. *Computers & Structures*, 48:22–32, 1993.

[4] P. J. Barendrecht. IsoGeometric Analysis for Subdivision Surfaces. Master's thesis, Technical University of Eindhoven, 2013.

[5] P. J. Barendrecht, M. Bartoň, and J. Kosinka. Efficient quadrature rules for subdivision surfaces in isogeometric analysis. *Comput. Methods Appl. Mech. Eng.*, 340:1–23, 2018.

[6] K.-P. Beier and Y. Chen. Highlight-line algorithm for realtime surface-quality assessment. *Comput.-Aided Des.*, 26(4):268–277, 1994.

[7] T. Belytschko, H. Stolarski, W. K. Liu, N. Carpenter, and J. SJ Ong. Stress projection for membrane and shear locking in shell finite elements. *Comput. Methods Appl. Mech. Eng.*, 51(1):221–258, 1985.

[8] D. Bommes, B. Lévy, N. Pietroni, E. Puppo, C. Silva, M. Tarini, and D. Zorin. State of the Art in Quad Meshing. In *Eurographics STARS*, 2012.

[9] V. Braibant and C. Fleury. Shape Optimal Design using B-splines. *Comput. Methods Appl. Mech. Eng.*, 44:247–267, 1984.

[10] E. Catmull and J. Clark. Recursively generated B-spline surfaces on arbitrary topological meshes. *Comput.-Aided Des.*, 10:350–355, 1978.

[11] P. Charrot and J. A. Gregory. A pentagonal surface patch for computer aided geometric design. *Comput. Aided Geom. Des.*, 1(1), 1984.

[12] F. Cirak, M. Ortiz, and P. Schröder. Subdivision surfaces: a new paradigm for thin-shell finite-element analysis. *Int. J. Numer. Meth. Engng.*, 47:2039–2072, 2000.

[13] CNN. Inside VW's high-tech transparent factory, 2014. `https://edition.cnn.com/2014/10/28/tech/gallery/industrial-art-inside-volkswagens-transparent-factory/index.html`.

[14] C. de Boor. B-form basics. In G. Farin, editor, *Geometric Modeling: Algorithms and New Trends*, pages 131–148. Society for Industrial and Applied Mathematics, 1987.

[15] T. DeRose, M. Kass, and T. Truong. Subdivision Surfaces in Character Animation. In *Proceedings of the ACM Conference on Computer Graphics (SIGGRAPH-98)*, pages 85–94. ACM Press, 1998.

[16] T. Dokken, T. Lyche, and K. F. Pettersen. Polynomial splines over locally refined box-partitions. *Comput. Aided Geom. Des.*, 30(3):331–356, 2013.

[17] D. Doo and M. Sabin. Behaviour of recursive division surfaces near extraordinary points. *Comput.-Aided Des.*, 10:356–360, 1978.

[18] G. Farin. *Curves and Surfaces for Computer Aided Geometric Design: A Practical Guide*. Academic Press Inc., 1988.

[19] Foundation Blender. Elephants Dream. `http://orange.blender.org`, 2006.

[20] C. Giannelli, B. Jüttler, and H. Speleers. THB-splines: The truncated basis for hierarchical splines. *Comput. Aided Geom. Des.*, 29(7):485–498, 2012.

[21] C. Gotsma. Rolling up our SLEFEs: Reflections on Putting an Academic Rendering Algorithm to Work, 2019. SIAM/GD 19.

[22] J. A. Gregory. Smooth interpolation without twist constraints. In R. E. Barnhill and R. F. Riesenfeld, editors, *Computer Aided Geometric Design*, pages 71–88. Academic Press Inc., 1974.

[23] J. A. Gregory and J. M. Hahn. Geometric continuity and convex combination patches. *Comput. Aided Geom. Des.*, 4(1-2):79–89, 1987.

[24] J. A. Gregory and J. M. Hahn. A C^2 polygonal surface patch. *Comput. Aided Geom. Des.*, 6(1):69–75, 1989.

[25] J. A. Gregory and J. Zhou. Filling polygonal holes with bicubic patches. *Comput. Aided Geom. Des.*, 11(4):391–410, 1994.

[26] D. Groisser and J. Peters. Matched G^k-constructions always yield C^k-continuous isogeometric elements. *Comput. Aided Geom. Des.*, 34:67–72, 2015.

[27] G. J. Hettinga, P. J. Barendrecht, and J. Kosinka. A Comparison of GPU Tessellation Strategies for Multisided Patches. In Olga Diamanti and Amir Vaxman, editors, *EG 2018 - Short Papers*. The Eurographics Association, 2018.

[28] G. J. Hettinga and J. Kosinka. Phong Tessellation and PN Polygons for Polygonal Models. In *EG 2017 - Short Papers*. The Eurographics Association, 2017.

[29] G. J. Hettinga and J. Kosinka. Multisided generalisations of Gregory patches. *Comput. Aided Geom. Des.*, 62:166–180, 2018.

[30] T. J. R. Hughes, J. A. Cottrell, and Y. Bazilevs. Isogeometric Analysis: CAD, Finite Elements, NURBS, Exact Geometry and Mesh Refinement. *Comput. Methods Appl. Mech. Eng.*, 194:4135–4195, 2005.

[31] W. Jakob, M. Tarini, D. Panozzo, and O. Sorkine-Hornung. Instant field-aligned meshes. *ACM Trans. Graph.*, 34(6):189, 2015.

[32] N. Jaxon and X. Qian. Isogeometric analysis on triangulations. *Comput.-Aided Des.*, 46:45–57, 2014.

[33] H. Kang, J. Xu, F. Chen, and J. Deng. A new basis for PHT-splines. *Graph. Models*, 82:149–159, 2015.

[34] K. Karčiauskas, A. Myles, and J. Peters. A C^2 Polar Jet Subdivision. In A. Scheffer and K. Polthier, editors, *Proceedings of Symposium of Graphics Processing (SGP), June 26-28 2006, Cagliari, Italy*, pages 173–180. ACM Press, 2006.

[35] K. Karčiauskas, T. Nguyen, and J. Peters. Generalizing bicubic splines for modelling and IGA with irregular layout. In *GDSPM 2015 in Salt Lake City, Utah October 12-14*, 2015.

[36] K. Karčiauskas, T. Nguyen, and J. Peters. Generalizing bicubic splines for modelling and IGA with irregular layout. *Comput.-Aided Des.*, 70:23–35, 2016.

[37] K. Karčiauskas, D. Panozzo, and J. Peters. T-junctions in spline surfaces. *ACM Trans. Graph.*, 36(5):170:1–9, 2017.

[38] K. Karčiauskas and J. Peters. Quad-net obstacle course. `http://www.cise.ufl.edu/research/SurfLab/shape_gallery.shtml`, accessed 2017-09-05.

[39] K. Karčiauskas and J. Peters. Bicubic polar subdivision. *ACM Trans. Graph.*, 26(4):14, 2007.

[40] K. Karčiauskas and J. Peters. Concentric Tesselation Maps and Curvature Continuous Guided Surfaces. *Comput. Aided Geom. Des.*, 24(2):99–111, 2007.

[41] K. Karčiauskas and J. Peters. Surfaces with Polar Structure. *Computing*, 79:309–315, 2007.

[42] K. Karčiauskas and J. Peters. Finite Curvature Continuous Polar Patchworks. In E. Hancock, R. R. Martin, and M. Sabin, editors, *IMA Mathematics of Surfaces XIII Conference*, pages 222–234, 2009.

[43] K. Karčiauskas and J. Peters. Lens-shaped surfaces and C^2 subdivision. *Computing*, 86(2):171–183, 2009.

[44] K. Karčiauskas and J. Peters. Biquintic G^2 surfaces via functionals. *Comput. Aided Geom. Des.*, pages 17–29, 2015.

[45] K. Karčiauskas and J. Peters. Can bi-cubic surfaces be class A? *Comput. Graph. Forum*, 34(5):229–238, 2015.

[46] K. Karčiauskas and J. Peters. Improved shape for multi-surface blends. *Graph. Models*, 8:87–98, 2015.

[47] K. Karčiauskas and J. Peters. Smooth multi-sided blending of biquadratic splines. *Computers & Graphics*, 46:172–185, 2015.

[48] K. Karčiauskas and J. Peters. Curvature continuous bi-4 constructions for scaffold- and sphere-like surfaces. *Comput.-Aided Des.*, 78:48–59, 2016.

[49] K. Karčiauskas and J. Peters. Minimal bi-6 G^2 completion of bicubic spline surfaces. *Comput. Aided Geom. Des.*, 41:10–22, 2016.

[50] K. Karčiauskas and J. Peters. Improved shape for refinable surfaces with singularly parameterized irregularities. *Comput.-Aided Des.*, 90:191–198, 2017.

[51] K. Karčiauskas and J. Peters. Refinable G^1 functions on G^1 free-form surfaces. *Comput. Aided Geom. Des.*, 54:61–73, 2017.

[52] K. Karčiauskas and J. Peters. Fair free-form surfaces that are almost everywhere parametrically C^2. *J. Comput. Appl. Math.*, pages 1–10, 2018.

[53] K. Karčiauskas and J. Peters. Rapidly contracting subdivision yields finite, effectively C^2 surfaces. *Computers & Graphics*, pages 1–10, 2018.

[54] K. Karčiauskas and J. Peters. Refinable bi-quartics for design and analysis. *Comput.-Aided Des.*, pages 1–10, 2018.

[55] K. Karčiauskas and J. Peters. High quality refinable G-splines for locally quad-dominant meshes with T-gons. *Comput. Graph. Forum*, 38(5):151–161, 2019.

[56] K. Karčiauskas and J. Peters. Localized G-splines for quad & T-gon meshes. *Comput. Aided Geom. Des.*, 71:244–254, 2019.

[57] K. Karčiauskas and J. Peters. Refinable smooth surfaces for locally quad-dominant meshes with T-gons. *Computers & Graphics*, 82:193–202, 2019.

[58] K. Karciauskas, J. Peters, and U. Reif. Shape Characterization of Subdivision Surfaces – Case Studies. *Comput. Aided Geom. Des.*, 21(6):601–614, 2004.

[59] P. Kiciak. Spline surfaces of arbitrary topology with continuous curvature and optimized shape. *Comput.-Aided Des.*, 45(2):154–167, 2013.

[60] R. Kraft. *Adaptive und linear unabhängige Multilevel B-Splines und ihre Anwendungen*. PhD thesis, University of Stuttgart, 1998.

[61] K. Li and X. Qian. Isogeometric analysis and shape optimization via boundary integral. *Comput.-Aided Des.*, 43(11):1427–1437, 2011.

[62] C. Loop. Second Order Smoothness over Extraordinary Vertices. In *SGP '04: Proceedings of the 2004 Eurographics/ACM SIGGRAPH symposium on Geometry processing*, pages 169–178. ACM Press, 2004.

[63] C. Loop and S. Schaefer. Approximating Catmull–Clark subdivision surfaces with bicubic patches. *ACM Trans. Graph.*, 27(1):8:1–8:11, 2008.

[64] C. T. Loop and T. D. DeRose. A Multisided Generalization of Bézier Surfaces. *ACM Trans. Graph.*, 8(3):204–234, 1989.

[65] C. T. Loop and S. Schaefer. G^2 Tensor Product Splines over Extraordinary Vertices. *Comput. Graph. Forum*, 27(5):1373–1382, 2008.

[66] C. T. Loop, S. Schaefer, T. Ni, and I. Castaño. Approximating subdivision surfaces with Gregory patches for hardware tessellation. *ACM Trans. Graph.*, 28(5), 2009.

[67] D. Lutterkort and J. Peters. Optimized Refinable Enclosures of Multivariate Polynomial Pieces. *Comput. Aided Geom. Des.*, 18(9):851–863, 2002.

[68] B. Marussig and T. J. R. Hughes. A Review of Trimming in Isogeometric Analysis: Challenges, Data Exchange and Simulation Aspects. *Arch. Comput. Methods Eng.*, 25(4):1059–1127, 2018.

[69] A. Myles, K. Karčiauskas, and J. Peters. Extending Catmull–Clark Subdivision and PCCM with Polar Structures. In *PG '07: Proceedings of the 15th Pacific Conference on Computer Graphics and Applications*, pages 313–320. IEEE Computer Society, 2007.

[70] A. Myles, K. Karčiauskas, and J. Peters. Pairs of bi-cubic surface constructions supporting polar connectivity. *Comput. Aided Geom. Des.*, 25(8):621–630, 2008.

[71] A. Myles and J. Peters. Bi-3 C^2 Polar Subdivision. *ACM Trans. Graph.*, 28(3), 2009.

[72] A. Myles and J. Peters. C^2 Splines Covering Polar Configurations. *Comput.-Aided Des.*, 43(11):1322–1329, 2011.

[73] T. Nguyen, K. Karčiauskas, and J. Peters. A comparative study of several classical, discrete differential and isogeometric methods for solving Poisson's equation on the disk. *Axioms*, 3(2):280–299, 2014.

[74] T. Nguyen, K. Karčiauskas, and J. Peters. C^1 finite elements on non-tensor-product 2d and 3d manifolds. *Appl. Math. Comput.*, 272(1):148–158, 2016.

[75] T. Nguyen and J. Peters. Refinable C^1 spline elements for irregular quad layout. *Comput. Aided Geom. Des.*, 43:123–130, 2016.

[76] S. J. Owen. A Survey of Unstructured Mesh Generation Technology. In *Proceedings of the 7th International Meshing Roundtable, IMR 1998, Dearborn, Michigan, USA, October 26-28, 1998*, pages 239–267, 1998.

[77] J. Peters. Parametrizing singularly to enclose vertices by a smooth parametric surface. In *Proceedings of Graphics Interface '91*, pages 1–7. Canadian Human-Computer Communications Society, 1991.

[78] J. Peters. Smooth interpolation of a mesh of curves. *Computing*, 7:221–247, 1991.

[79] J. Peters. Smooth free-form surfaces over irregular meshes generalizing quadratic splines. *Comput. Aided Geom. Des.*, 10:347–361, 1993.

[80] J. Peters. PN Quads. Technical report, University of Florida, CISE, 2000.

[81] J. Peters. Geometric Continuity. In *Handbook of Computer Aided Geometric Design*, pages 193–229. Elsevier, 2002.

[82] J. Peters. On refinable tri-variate C^1 splines for box-complexes including irregular points and irregular edges. In *Mathematical Foundations of Isogeometric Analysis*, volume 33, pages 33–35. Mathematisches Forschungsinstitut Oberwolfach, 2019.

[83] J. Peters and K. Karčiauskas. An introduction to guided and polar surfacing. In *Mathematical Methods for Curves and Surfaces. 7th International Conference on Mathematical Methods for Curves and Surfaces (Toensberg, 2008)*, volume 5862 of *Lecture Notes in Computer Science*, pages 299–315. Springer, 2010.

[84] J. Peters and U. Reif. *Subdivision Surfaces*, volume 3 of *Geometry and Computing*. Springer, 2008.

[85] J. Peters and X. Wu. On the optimality of piecewise linear max-norm enclosures based on slefes. In *Curve and surface design: Saint Malo 2002*, Modern Methods in Mathematics. Nashboro Press, 2003.

[86] J. Peters and X. Wu. Sleves for planar spline curves. *Comput. Aided Geom. Des.*, 21(6):615–635, 2004.

[87] Pia R. Pfluger and Marian Neamtu. On degenerate surface patches. *Numer. Algorithms*, 5(11):569–575, 1993.

[88] H. Prautzsch. Freeform splines. *Comput. Aided Geom. Des.*, 14(3):201–206, 1997.

[89] N. Ray, W. C. Li, B. Lévy, A. Sheffer, and P. Alliez. Periodic Global Parameterization. *ACM Trans. Graph.*, 25(4):1460–1485, 2006.

[90] U. Reif. Turbs—topologically unrestricted rational B-splines. *Constr. Approx.*, 14(1):57–77, 1998.

[91] M. Sabin. Transfinite Surface Interpolation. In Glen Mullineux, editor, *Mathematics of Surfaces*, volume VI, pages 517–534. Clarendon Press, 1996.

[92] P. Salvi and T. Várady. Multi-sided Bézier surfaces over concave polygonal domains. *Computers & Graphics*, 74:56–65, 2018.

[93] G. Sangalli, T. Takacs, and R. Vazquez. Unstructured spline spaces for isogeometric analysis based on spline manifolds. *Comput. Aided Geom. Des.*, 47:61–82, 2016.

[94] U. Schramm and W. D. Pilkey. The coupling of geometric descriptions and finite elements usin+++g NURBS - A study in shape optimization. *Finite Elem. Anal. Des.*, 340:11–34, 1993.

[95] L. L. Schumaker and M.-J. Lai. *Spline Functions on Triangulations*. Cambridge University Press, 2007.

[96] T. W. Sederberg, J. Zheng, A. Bakenov, and A. Nasri. T-splines and T-NURCCs. In Jessica Hodgins and John C. Hart, editors, *Proceedings of ACM SIGGRAPH 2003*, pages 477–484. ACM Press, 2003.

[97] K.-L. Shi, J.-H. Yong, L. Tang, J.-G. Sun, and J.-C. Paul. Polar NURBS Surface with Curvature Continuity. *Comput. Graph. Forum*, 32(7):363–370, 2013.

[98] Y. K. Shyy, C. Fleury, and K. Izadpanah. Shape Optimal Design using higher-order elements. *Comput. Methods Appl. Mech. Eng.*, 71:99–116, 1988.

[99] J. Smith and S. Schaefer. Selective Degree Elevation for Multi-Sided Bézier Patches. *Comput. Graph. Forum*, 34(2):609–615, 2015.

[100] T. Várady, A. P. Rockwood, and P. Salvi. Transfinite surface interpolation over irregular n-sided domains. *Comput.-Aided Des.*, 43(11):1330–1340, 2011.

[101] T. Várady, P. Salvi, and G. Karikó. A Multi-sided Bézier Patch with a Simple Control Structure. *Comput. Graph. Forum*, 35(2):307–317, 2016.

[102] A. Vaxman, M. Campen, O. Diamanti, D. Panozzo, D. Bommes, K. Hildebrandt, and M. Ben-Chen. Directional Field Synthesis, Design, and Processing. In *SIGGRAPH '17: ACM SIGGRAPH 2017 Courses*. ACM Press, 2016.

[103] A. Vlachos, J. Peters, C. Boyd, and Jason L. Mitchell. Curved PN Triangles. In *Symposium on Interactive 3D Graphics*, Bi-Annual Conference Series, pages 159–166. ACM Press, 2001.

[104] X. Wang and X. Qian. An optimization approach for constructing trivariate B-spline solids. *Comput.-Aided Des.*, 46:179–191, 2014.

[105] Wikipedia contributors. Class_A_surfaces. `http://en.wikipedia.org/wiki/Class_A_surfaces`, accessed Jan 2017.

[106] Wikipedia contributors. Freeform surface modelling — Wikipedia, The Free Encyclopedia, 2018. https://en.wikipedia.org/w/index.php?title=Freeform_surface_modelling&oldid=871471382, accessed 2018-12-31.

[107] Y. Yamada. *Clay Modeling: Techniques for giving three-dimensional form to idea*. Nissan Design Center, Kaneko Enterprises, 1997.

[108] P. Yang and X. Qian. A B-spline-based approach to heterogeneous objects design and analysis. *Comput.-Aided Des.*, 39(2):95–111, 2007.

[109] X. Ye. Curvature continuous interpolation of curve meshes. *Comput. Aided Geom. Des.*, 14(2):169–190, 1997.

[110] Y. In Yeo, S. Bhandare, and J. Peters. Efficient Pixel-accurate Rendering of Animated Curved Surfaces. In *8th International Conference on Mathematical Methods for Curves and Surfaces, Oslo June 2012*, volume 8177 of *Lecture Notes in Computer Science*, pages 491–509. Springer, 2014.